

# Three-Dimensional Investigation of the Pore Space in Carbon Preforms of Metal Infiltrated Carbon Based Silicon Carbide Ceramics

Raouf Jemmali <sup>a,\*</sup>, Steffen Weber <sup>a</sup>, Dietmar Koch <sup>a</sup>

<sup>a</sup> German Aerospace Center (DLR), Institute of Structures and Design, 70569 Stuttgart, Germany

\* Corresponding author. Tel.: +49-711-6862-453; fax: +49-711-6862-227;

E-Mail address: raouf.jemmali@dlr.de

## Abstract:

The microstructures of MiCaSiC<sup>®</sup> ceramics (Metal Infiltrated Carbon based Silicon Carbide) depend among others on the pore space properties of the carbon preforms before the liquid silicon infiltration (LSI). The aim of this work was to obtain three-dimensional information of the complex and non-homogeneous pore network in the carbon preform using microfocus X-ray computed tomography ( $\mu$ CT) and adequate image processing algorithms. It was found that it is possible to identify the optimum silicon infiltration direction by analyzing the porosity profiles. The pore size distribution was derived from the tomographic images using granulometry and cells reconstruction methods. Both results were compared with the distribution

provided experimentally by the mercury intrusion porosimetry (MIP). Some relevant structural parameters (e.g. geometrical tortuosity, surface density, etc.) were calculated from the tomograms. A representative unit cell (RUC) was derived on the basis of those values. This information will reduce the computational efforts when performing  $\mu$ CT data based simulations, in order to better understand the LSI process for MiCaSiC<sup>®</sup>.

## Keywords:

MiCaSiC<sup>®</sup>, Silicon carbide (SiC), microfocus X-ray computed tomography ( $\mu$ CT); liquid silicon infiltration (LSI); ceramics; pore size distribution; representative unit cell (RUC)

## 1. Introduction

Silicon carbide based ceramics (SiC) have favorable thermal, mechanical and chemical characteristics. That is why SiC ceramics are attractive candidates for the use as structural components in many application fields. Commercially available SiC ceramics are mainly produced by cost intensive sintering methods which require high process energies and expensive SiC powders as raw materials [1]. In this context, one opportunity to reduce costs is the use and manufacture of metal infiltrated carbon based ceramics (MiCaSiC<sup>®</sup>). This material has several advantages, such as the cost-effective formation of silicon carbide and the possibility of near-shape production of components in contrast to sintered materials. The development of MiCaSiC<sup>®</sup> ceramics comprised challenges like raw material and processing research. Thereby, the targeted conversion of carbon to SiC ceramics with specifically adjusted material characteristics is a key factor. It is possible to adapt MiCaSiC<sup>®</sup> to further commercially or totally new industrial applications by regulating the material phases and properties. Therefore the accurate knowledge of the pore space properties before the silicon infiltration process of the carbon preforms is necessary.

In general, a porous structure can be described by means of several characteristics such as open/closed porosity values, pore size distribution and connectivity between the pores. These parameters have an important effect on physical properties of a porous medium such as permeability to gas or fluid flow, electrical conductivity and acoustic absorption [2]. A powerful non-destructive technique to provide the direct 3D representation of pore space in carbon preforms is the microfocus X-ray computed tomography

( $\mu$ CT). This approach is merely limited by the machine resolution, currently around 1 $\mu$ m. Hence, sub-micron sized pores in carbon preforms cannot be detected. The features in the range of few nanometers up to one micron can be imaged by other well established 2D imaging techniques such as light and electron microscopy with appropriate image processing software. The pore size distribution can be measured experimentally by intrusion methods such as mercury porosimetry or gas pycnometry. In turn, these widely used techniques don't provide any 3D morphological information of the material and pore space phases. Aside from the resolution limitation,  $\mu$ CT combines the advantages of both microscopic and physical procedures. Many recent works has occurred in the field of the 3D characterization of pore networks of different materials using  $\mu$ CT data. To the best of our knowledge there are no results in the literature regarding the investigation of the influence of the complex pore networks on the microstructures of silicon carbide based ceramics produced via liquid silicon infiltration process (LSI).

The present paper introduces two useful methods for the calculation of pore size distribution (PSD) on the basis of high resolution microfocus X-ray computed tomography data. In addition, structural parameters (e.g. geometrical tortuosity, surface density, etc.) are calculated and used for the determination of a representative unit cell (RUC). The knowledge of the RUC will reduce effectively the numerical effort when performing simulations (e.g. calculation of the absolute permeability) based on exact geometries extracted from  $\mu$ CT data in order to better understand the reaction mechanisms during the silicon infiltration process. Properties such as permeability and conductivity can be

numerically simulated either directly on the obtained 3D CT representation or after extraction of an equivalent topological network. An overview about relevant works is given in [3]. Such simulations will be conducted in future studies.

## 2. Materials and Methods

### 2.1 Manufacturing of MiCaSiC®-Samples

The manufacture route of MiCaSiC® ceramics is a three stage process, which is schematically shown in Fig. 1. The first step includes the green body shaping process. This can proceed through various methods such as warm pressing, extrusion, injection molding or additive manufacturing as well. After green body manufacture a pyrolysis is carried out to create a highly porous carbon preform. In the last process step the carbon preform is infiltrated with liquid silicon (via LSI process) to form a dense silicon carbide based ceramic.

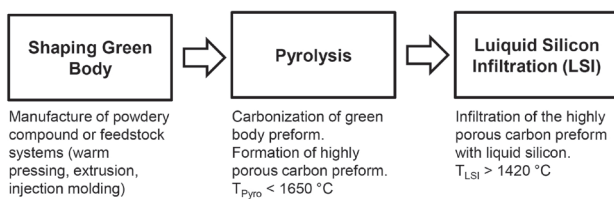


Fig. 1. The manufacture route of MiCaSiC® ceramics.

To investigate the three dimensional pore evolution in carbon preforms of MiCaSiC® ceramics after the pyrolysis, one material type were produced by warm pressing and associated pyrolysis. Fig. 2a demonstrates the complexity of the pore morphology of the investigated carbon preform. A typical final microstructure of MiCaSiC® is shown in Fig. 2b. The three material constituents of the final product are carbon (C), silicon carbide (SiC) and silicon (Si).

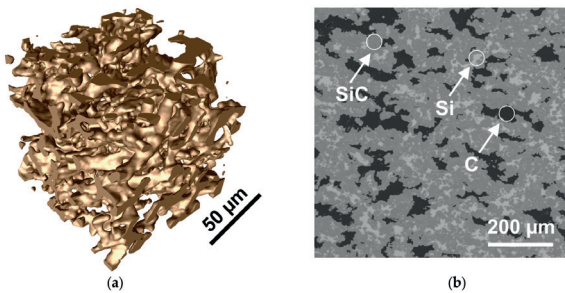


Fig. 2. (a): 3D surface rendering of the highly complex pore network in a sub-volume from the reconstructed μCT data set; (b): SEM image of a typical microstructure of MiCaSiC®.

### 2.2 X-Ray micro-computed tomography

The microfocus computed tomography (μCT) scan was conducted using a high resolution μCT-System (nanotom, GE Sensing & Inspection Technologies GmbH, Wunstorf) consisting of a microfocus X-ray tube with a maximum accelerating voltage of 180 kV and a 12-bit flat panel detector (active area 2348 x 2348 pixels at 50 microns per pixel). The setup is illustrated in Fig. 3. The μCT scan was performed with the X-ray parameters 80 kV/180 μA at an expo-

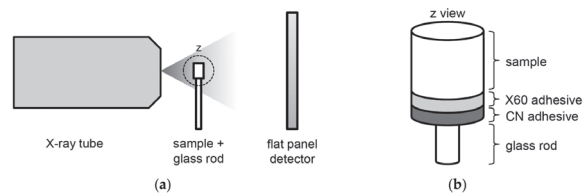


Fig. 3. μCT measurement setup [12]: in (a) the main components are shown: X-ray tube, specimen with sample holder and detector; the attachment of the carbon preform specimen to the glass rod via two adhesive types is sketched in (b).

sure time of 600 ms. A voxel size of 1 μm could be achieved. The so acquired 2D X-ray images were reconstructed with a special reconstruction algorithm known as Filtered Back Projection. The μCT data were visualized and analyzed with the software packages VGStudioMax 2.2 (Volume Graphics, Heidelberg) and MAVI 1.5.2 (Fraunhofer IWTM, Kaiserslautern).

A cylindrical specimen with a diameter of 5 mm and a height of 10 mm was extracted from the middle of the manufactured plates in order to avoid border effects which might result from the warm pressing during the green body shaping. As sample holder we used a rod made of borosilicate glass with a diameter of 3 mm because of its quite low coefficient of thermal expansion. This is important to prevent sample drifts due to the thermal expansion of the sample holder due the heat formation around the investigated sample. A cyanoacrylate superglue (CN, preusser-messtechnik GmbH, Bergisch Gladbach) was used to fix the specimen to the glass rod. To avoid the infiltration of the pore network with this very low viscosity CN and consequently wrong results, we had to seal the bottom of the specimen. For this purpose we used a two component adhesive (X60, HBM Darmstadt).

### 2.3 Experimental porosity measurement

In order to experimentally verify the porosity results obtained via CT, two methods were used: Archimedes water infiltration (according to DIN EN 993-1) and Mercury intrusion porosimetry (MIP). The MIP system used is a Pascal 140/240 (Thermo Scientific, Germany). The pressure range was 0-200 MPa. This pressure range corresponds to pore sizes from 100μm (low pressure) to 10nm (high pressure). The pore sizes were calculated with a cylindrical and plate pore shape model and an assumed contact angle of mercury of 140°.

### 2.4 Structural parameters

In this work, structural parameters are defined as those morphological key values enabling the characterization of the pore network in carbon preforms of MiCaSiC® ceramics. The first important and easy to determine parameter is the total porosity ε in percent, and is defined as:

$$\epsilon = \frac{V_p}{V_T} \cdot 100 \quad (1)$$

where  $V_p$  and  $V_T$  are the volumes of pore space and the total volume of the reconstructed μCT volume, respectively. They are determined by counting the voxels of the corresponding phase.

Another important structural parameter for porous materials is the geometrical tortuosity  $\tau$ . It helps understanding the mechanism of fluid flow through complex void spaces [4]. Usually, the tortuosity  $\tau$  is defined by [5, 6]:

$$\tau = \frac{L_e}{L} \quad (2)$$

where  $L_e$  is the total flow path length and  $L$  is the shortest distance between defined starting and ending points, therefore  $\tau \geq 1$ . Higher values of  $\tau$  indicate longer, more complex and twisted path thus making the fluid flow more difficult.

The surface density (SV) in mm<sup>-1</sup>, also called specific surface area, might be a significant characteristic for later investigations on the reactivity of carbon based materials. For carbon preforms we define it as:

$$S_V = \frac{CS}{CV} \quad (3)$$

where  $C_V$  (mm<sup>3</sup>) is the carbon volume and  $C_S$  (mm<sup>2</sup>) is the carbon surface. The surface is the boundary between carbon and pore space, the volume of the carbon is enclosed by the surface. The surface density is thus a measure for the carbon surface per given carbon volume.

A central parameter to determine the connectivity of the pores is the Euler number  $\chi$ , also known as the Euler-Poincaré characteristic [7]. This number is a characteristic for the connectedness of the pore network: positive values indicate bad connected pores, while negative values point to better connection [8]. For a realistic comparison between different volumes, we divide the Euler number  $\chi$  by the total volume  $V_T$  in mm<sup>3</sup> to obtain the specific Euler number  $\chi_V$  in mm<sup>-3</sup>:

$$\chi_V = \frac{\chi}{V_T} \quad (4)$$

### 3. Results and discussion

The noise contained in the reconstructed tomographic images makes a further processing difficult. Hence, an adequate image enhancing technique must be selected. We used a nonlinear filter, the median filter, which is dedicated to minimize the noise while preserving the edges [9]. Fig. 4a shows the grey values histogram before and after median filtering, respectively as a filled grey surface and a black curve. After noise reduction, two different peaks in the histogram can be distinguished. This bimodal grey values distribution fits two phases in the specimen, pore space and carbon phase. For further data analysis, it is necessary to

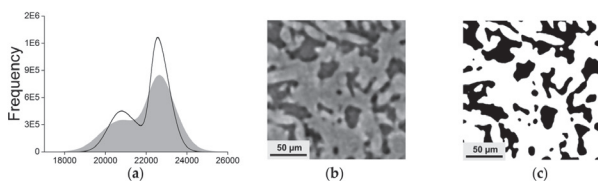


Fig. 4. In (a) the  $\mu$ CT histogram of the reconstructed volume  $1.3 \times 1.3 \times 1.3 \text{ mm}^3$  is plotted as a filled grey surface, the two material phases which are pore and solid cannot be separated because of the noisy images. After application of the median filter, the grey values histogram turns into a bimodal distribution (black curve), where two peaks can be distinguished easily. The binarized image after segmentation of (b) using the Otsu's threshold method is shown in (c).

classify the volume pixels either in void or solid. This step is called segmentation. There are several global and local segmentation algorithms in the literature [10]. In the present work we used the Otsu's threshold method [11] for mainly two reasons. First, it is suitable for data sets with bimodal grey value distributions. Second, it is user independent, since it is based on statistical calculations. The result of the Otsu's segmentation applied on the already filtered image (Fig. 4b) is a binary image as shown in Fig. 4c.

After the CT data segmentation in solid and pore phases, the total porosity in the reconstructed volume  $1300^3$  voxels was calculated. The porosity value obtained from the CT images was in very good agreement with the results achieved by the Archimedes and mercury intrusion porosimetry measurements. The results are reported in Table 1.

**Table 1. Porosity values obtained with Archimedes, mercury intrusion porosimetry and  $\mu$ CT.**

Method	Total porosity (%)
Archimedes	53.1
Mercury Intrusion porosimetry	51.4
$\mu$ CT	50.2

The fluctuation of the porosity along the sample depth is investigated. The 2D porosity value was calculated for each CT slice in all three directions x, y and z. The results are plotted in Fig. 5 as area fraction profiles (AFP). The porosity values fluctuate between 47.5% and 52% in x, 47% and 52% in y and between 49% and 52% in z direction. The overall porosity value for the analysed volume of  $1.3^3 \text{ mm}^3$  is 50.2%. The third AFP (z-direction) which corresponds to the warm pressing direction exhibits the most stable trend. This might result later during the last manufacturing stage (siliconization) in a more homogeneous silicon infiltration along the z-direction.

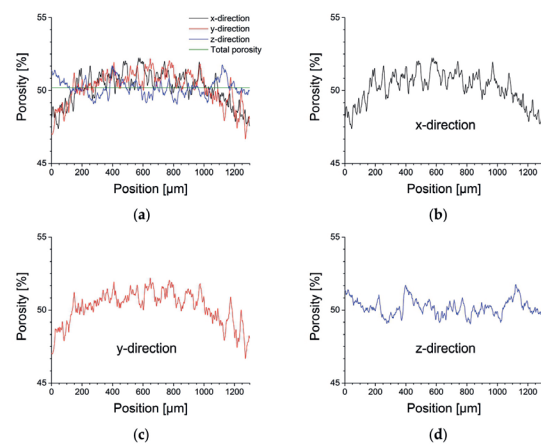


Fig. 5. Porosity fluctuation in a reconstructed  $\mu$ CT volume (size  $1.3 \times 1.3 \times 1.3 \text{ mm}^3$ ) of the carbon preform. The area fraction profiles (AFP) of the pore phase are plotted as a function of the sample depth in (a) for all the three directions x, y, and z. The average porosity value 50.2% is displayed as horizontal line. The single AFPs are separately shown in x (b), y (c) and z-direction (d).

The segmented 3D data was also used to characterize the pore networks in the carbon preforms in terms of pore size distribution. First, it has to be underlined that the amount

of closed pores which can be detected with the known CT scan resolution is negligible, as it has been shown in a prior work [12]. It means that almost all pore channels are connected together. This high degree of connectivity is indicated by the negative high value of the specific Euler number around  $-2 \cdot 10^{14} \text{ mm}^{-3}$ . We used two different approaches to examine the pore size distributions: the spherical granulometry and the cells reconstruction. The granulometry [13] uses morphological openings with a structuring element (in this work a sphere) to compute a grain or pore size distribution in binary images. For each voxel in the background the diameter of the maximal inscribed sphere in the pore channel is calculated. The cumulative distribution of all diameters is a granulometric curve as shown in Fig. 4(c). The granulometry is a reliable and repeatable tool since it is user independent, in spite of the time consuming computation.

The second method used for the determination of the pore size distribution is based on cells reconstruction. The image background, which represents the pore space, is segmented into isolated regions or cells. Therefore, its result can be interpreted as a discrete pore size distribution. Each cell is then assigned to a sphere with an equivalent volume. This procedure uses basically the watershed algorithm and some additional image processing techniques (e.g. filtering, separation, labelling) that require specific input parameters (e.g. threshold values). These are estimated according to a subjective plausibility approximation done by the user. Thus, the pore distribution resulting from cells reconstruction depends considerably on the choice of these parameters. Fig. 6 shows the output images of both methods in the same representative  $\mu\text{CT}$  slice.

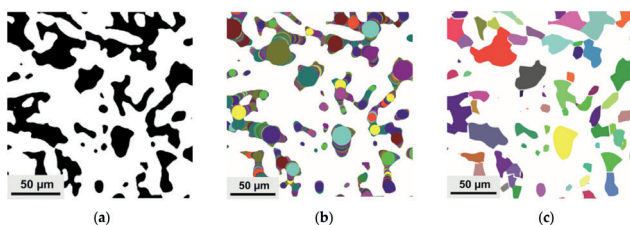


Fig. 6. Results from granulometry and reconstructed cells methods shown in a single  $\mu\text{CT}$  slice. The colors are defined arbitrarily and serve just for better visualization. The binarized image is shown in (a). In the granulometric image of the same slice (b), cross sections of the maximal inscribed spheres are visible. The isolated regions determined with the cells reconstruction method are displayed in (c).

The pore size distributions from granulometry and cells reconstruction were calculated for a volume of  $1300^3$  voxels and plotted in Fig. 7a. To simplify the histograms, the diameters ranges are binned in  $5\mu\text{m}$  intervals. The shapes of both distributions show a certain similarity, although they are based on two different computation algorithms. The pore size distribution measured by means of mercury intrusion porosimetry (MIP) shown in Fig. 7b, reveals a monomodal shape. The high peak represents a modal diameter range between  $4.6$  and  $6.3\mu\text{m}$  (median value is  $4.8\mu\text{m}$ ). The average pore diameter is  $215\text{ nm}$ . These results differ strongly from those obtained from the methods based on the  $\mu\text{CT}$  data (granulometry and cells reconstruction) where sub-micrometer pores cannot be detected due to the resolution limitation of the used  $\mu\text{CT}$  system. On the

other hand, their results reveal significantly higher pore sizes than the mercury intrusion porosimetry. In order to better compare all three results, the cumulative pore size distributions were calculated and plotted in Fig. 7c. It has to be emphasized that the MIP pore diameter values below  $4\mu\text{m}$  were neglected, since these cannot be detected by  $\mu\text{CT}$ . The granulometry and cells reconstruction curves show here an identical shape with a horizontal offset of about  $3\mu\text{m}$ . The third curve (mercury intrusion porosimetry) has a totally different shape for the already mentioned reasons.

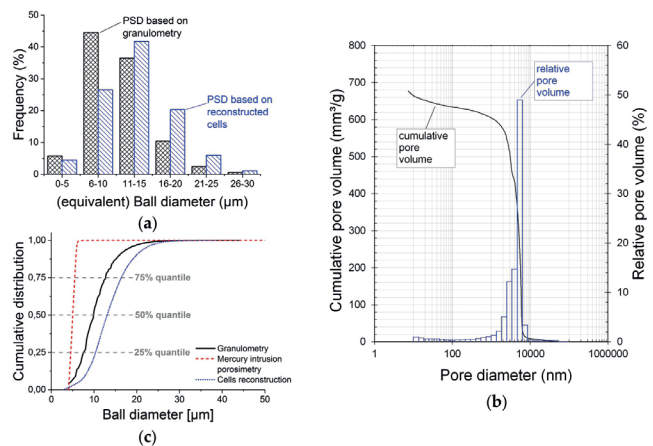


Fig. 7. Results from granulometry and reconstructed cells methods shown in a single  $\mu\text{CT}$  slice. The colors are defined arbitrarily and serve just for better visualization. The binarized image is shown in (a). In the granulometric image of the same slice (b), cross sections of the maximal inscribed spheres are visible. The isolated regions determined with the cells reconstruction method are displayed in (c).

To better quantify this deviation, the quantile values (at 25%, 50% and 75%) were calculated. The results are summarized in Table 2. For instance, 75% of the pores are below  $14.7\mu\text{m}/16.4\mu\text{m}$  for respectively granulometry and cells reconstruction. In contrast, the MIP reveals a much lower 75% quantile of  $5.5\mu\text{m}$ .

Table 2. Pore diameter quantile values.

Quantile	Granulometry	Cells reconstruction	MIP
25%	$7.5\mu\text{m}$	$10\mu\text{m}$	$4.5\mu\text{m}$
50%	$9.9\mu\text{m}$	$13\mu\text{m}$	$5\mu\text{m}$
75%	$12.7\mu\text{m}$	$16.4\mu\text{m}$	$5.5\mu\text{m}$

The pore diameters ( $d_p$ ) in MIP are calculated by means of the Washburn equation [14]:

$$d_p = -2 \frac{\gamma \cdot \cos \theta}{p}$$

where  $\gamma$  is the surface tension of the non-wetting phase mercury,  $\theta$  is the contact angle and  $p$  the required pressure to force mercury to enter a capillary.

The high discrepancy between MIP and 3D analysis is explained by Holzer et. al. [15] with the ink-bottle effect [16]. Their argumentation states concisely that the needed pressure values are very high when large pores are filled during the mercury intrusion over narrow pore necks. This leads

**Table 3. Structural parameters values for six reconstructed volumes with different edges lengths.**

Structural Parameter	Cube edge length (CEL) of the reconstructed volume (mm)					
	0.1	0.2	0.4	0.7	1.0	1.3
Total porosity $\varepsilon$ (%)	52.6	54.7	51.4	51.3	50.9	50.2
Geometrical tortuosity $\tau$ (-) in:	x	1.08	1.08	1.07	1.07	1.06
	y	1.11	1.10	1.07	1.07	1.07
	z	1.09	1.09	1.07	1.06	1.06
Surface density $S_v$ ( $\times 10^4$ mm <sup>-1</sup> )	14.65	14.28	13.72	13.67	13.65	13.63
Specific Euler number $\chi_v$ ( $\times 10^{14}$ mm <sup>-3</sup> )	-2.70	-2.37	-1.85	-1.83	-1.83	-1.86

to an over-estimation of the very small pores. In this case the Washburn equation, where the pressure required for the mercury to intrude the capillary is inversely proportional to its diameter, is no longer valid. The  $\mu$ CT data based pore size distributions are more realistic, because the pore sizes can be verified by measuring them directly in the tomograms.

The variation of all structural parameters described in the section “Materials and Methods” in function of the volume size is investigated. The main purpose is to find out whether and for which volume sizes these values become constant. For this purpose, seven concentric volumes of interest (VOI) were reconstructed from the same CT scan. The cube edge lengths (CEL) are respectively 0.1 mm, 0.2 mm, 0.4 mm, 0.7 mm, 1.0 and 1.3 mm. The central structural parameters porosity  $\varepsilon$ , geometrical tortuosity  $\tau$ , surface density  $S_v$  and specific Euler number  $\chi_v$  were calculated for all VOIs. The results are summarized Table 3 and plotted in Fig. 8.

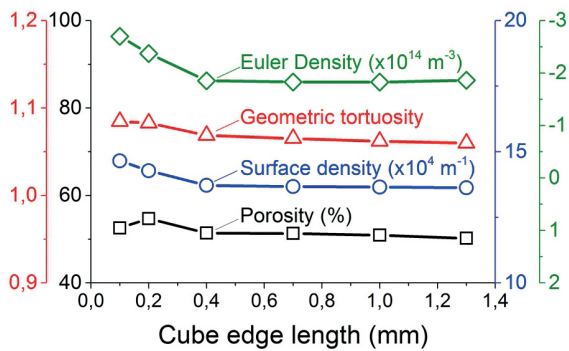


*Fig. 8. Calculated structural parameters as functions of different volumes of interest (VOI) with cube edge lengths (CEL) between 0.1 and 1.3 mm [17]. The VOIs with CEL between 0.4 and 1.3 mm show constant curves for all four parameters. In this range a representative unit cell (RUC) seems to be suitable.*

It can be observed that the curves are constant for the cube edge lengths between 0.4 and 1.3 mm. A higher deviation can be seen at 0.1 and 0.2 mm. Thus, it can be deduced that a representative unit cell (RUC) can be chosen in the range between 0.4 and 1.3 mm in terms of the investigated structural parameters and for this material type. This information will be very useful when conducting in later

researches simulations based on the real model extracted from the high resolution  $\mu$ CT data. Then it can be assumed that a cube with an edge length of 0.4 mm will yield to the same results as another with 1.3 mm. The bigger the volume, the higher is the number of the mesh elements (e.g. tetrahedrons) that must be created. Thus, the  $\mu$ CT based simulations would be possible and the computational effort would be highly reduced.

**4. Conclusions**

The microfocus computed tomography ( $\mu$ CT) with appropriate image processing algorithms is a powerful imaging and non-destructive tool for the quantitative three-dimensional description of the pore networks in MiCaSiC® carbon preforms.

In this study, we have presented some relevant 3D structural parameters which reflect the morphology and connectedness of the pores in the investigated material. We have calculated these parameters for  $\mu$ CT volumes between 0.2<sup>3</sup> mm<sup>3</sup> and 1.3<sup>3</sup> mm<sup>3</sup>. We found that the values are quite constant for volumes above 0.4<sup>3</sup> mm<sup>3</sup>. A representative unit cell (RUC) can be selected in this range. We will use this finding in future studies as a basis for real structure based simulations.

We have also shown that the determination of the porosity area fraction profiles can be used to predict the adequate positioning of the carbon preforms during the silicon infiltration process.

We have used two 3D image based approaches to determine the pore size distribution in the complex pore channels of the MiCaSiC® carbon preforms: spherical granulometry and cells reconstruction. Both showed similar results, but differ strongly from the mercury intrusion porosimetry which is affected by the ink-bottle-effect. In further works, we will create 3D pore models of the investigated material by using advanced methods such as skeletonizing algorithms.

**Acknowledgments**

This research was supported by German Aerospace Center, Institute of Structures and Design, Stuttgart, Germany. The authors gratefully acknowledge Mrs. Gudrun Steinhilber for conducting the mercury intrusion porosimetry measurements.

## References

- [1] S. Weber, *Entwicklung und Herstellung von MiCaSiC-Keramiken über die Flüssigphaseninfiltration von komplexen und neuartigen Kohlenstoffstrukturen*, Universität Stuttgart, 2016, p. 213.
- [2] R.C. Acharya, S.E.A.T.M. van der Zee, A. Leijnse, *Porosity–permeability properties generated with a new 2-parameter 3D hydraulic pore-network model for consolidated and unconsolidated porous media*, *Advances in Water Resources* 27(7) (2004) 707-723.
- [3] A.S. Al-Kharusi, M.J. Blunt, *Multiphase flow predictions from carbonate pore space images using extracted network models*, *Water Resources Research* 44(6) (2008) n/a-n/a.
- [4] R. Vallabh, P. Banks-Lee, A.-F. Seyam, *New approach for determining tortuosity in fibrous porous media*, *Journal of Engineered Fibers and Fabrics* 5(3) (2010) 7-19.
- [5] J. Bear, *Dynamics of fluids in porous media*, American Elsevier Pub. Co., New York, 1972.
- [6] P.C. Carman, *Flow of gases through porous media*, Butterworths Scientific Publications, London, 1956.
- [7] A. Odgaard, *Three-dimensional methods for quantification of cancellous bone architecture*, *Bone* 20(4) (1997) 315-328.
- [8] H.-J. Vogel, *Topological Characterization of Porous Media*, in: K. Mecke, D. Stoyan (Eds.), *Morphology of Condensed Matter: Physics and Geometry of Spatially Complex Systems*, Springer Berlin Heidelberg, Berlin, Heidelberg, 2002, pp. 75-92.
- [9] A.R. Sawant, H.D. Zeman, D.M. Muratore, S.S. Samant, F.A. DiBianca, *Adaptive median filter algorithm to remove impulse noise in x-ray and CT images and speckle in ultrasound images*, 1999, pp. 1263-1274.
- [10] J. Ohser, K. Schladitz, *3D images of materials structures : processing and analysis*, Wiley-VCH, Weinheim, 2009.
- [11] N. Otsu, *Threshold selection method from gray-level histograms*, *IEEE Trans Syst Man Cybern SMC-9(1)* (1979) 62-66.
- [12] S. Weber, R. Jemmali, D. Koch, H. Voggenreiter, *Microstructures and physical properties of biomorphic SiSiC ceramics manufactured via LSI-technique*, *Advances in Bioceramics and Porous Ceramics V: Ceramic Engineering and Science Proceedings, Volume 33 (6)* (2012) 105.
- [13] G. Matheron, *Random sets and integral geometry*, Wiley 1975.
- [14] E.W. Washburn, *The Dynamics of Capillary Flow*, *Physical Review* 17(3) (1921) 273-283.
- [15] L. Holzer, F. Indutnyi, P.H. Gasser, B. Münch, M. Wegmann, *Three-dimensional analysis of porous BaTiO<sub>3</sub> ceramics using FIB nanotomography*, *Journal of Microscopy* 216(1) (2004) 84-95.
- [16] F. Moro, H. Böhni, *Ink-Bottle Effect in Mercury Intrusion Porosimetry of Cement-Based Materials*, *Journal of Colloid and Interface Science* 246(1) (2002) 135-149.
- [17] R. Jemmali, S. Weber, D. Koch, *Characterization of complex pore networks in carbon preforms of MiCa-SiC ceramics on the basis of X-ray computed tomography*, *Industrial CT Scanning*, DIT (Danish Institute of Technology) Munich, 2013.